Ecological Research

WILEY

RESEARCH ARTICLE OPEN ACCESS

Detection of Heat and Drought Effects on the Photosynthetic Activity Using Solar-Induced Chlorophyll Fluorescence and a Photochemical Reflectance Index in a Cool-Temperate Larch Forest in Japan

Tomoki Morozumi[1] | Tomomichi Kato[2] | Hideki Kobayashi[3] | Yoshiyuki Takahashi[1] | Hibiki M. Noda[1]

[1]Earth System Division, National Institute for Environmental Studies, Tsukuba, Ibaraki, Japan | [2]Research Faculty of Agriculture, Hokkaido University, Sapporo, Hokkaido, Japan | [3]Institute of Arctic Climate and Environment Research, Japan Agency for Marine-Earth Science and Technology (JAMSTEC), Yokohama, Kanagawa, Japan

Correspondence: Tomoki Morozumi (morozumi.tomoki@nies.go.jp)

Received: 27 August 2025 | **Revised:** 25 March 2026 | **Accepted:** 1 April 2026

Keywords: chlorophyll fluorescence | drought response | remote sensing | stomatal regulation | tower flux

ABSTRACT

Recent frequent heatwaves have adversely affected the carbon cycles of terrestrial ecosystems. Solar-induced chlorophyll fluorescence (SIF) and the photochemical reflectance index (PRI) can detect heat and drought stress in vegetation. However, the applicability of these indicators in extreme cases, such as heatwaves, needs consideration. We examined diurnal changes observed in tower-based SIF, PRI, canopy conductance, and gross primary productivity (GPP) over 3 weeks during mid-summer in 2022 in a cool-temperate deciduous forest covered by *Larix kaempferi* (Lamb.) Carrière, in Japan. We found that half-hourly GPP and SIF declined significantly from noon to afternoon during the latter part of clear, extremely hot days (up to 31°C) when the soil water content (SWC) was low (< 21%), and the vapor pressure deficit (VPD) was high (> 15 hPa). Values of GPP and SIF peaked at 21.7°C and 26.8°C, respectively, and they declined at higher temperatures. Canopy conductance declined with increasing air temperature and VPD, suggesting that stomatal closure caused the observed reduction in GPP. To investigate the stress response without light-dependent variations, canopy fluorescence emission efficiency (εF) and light use efficiency (LUE) were calculated from SIF and GPP, respectively. VPD had the most significant negative correlation with PRI, LUE, and εF. εF was also associated with SWC, particularly under lower SWC conditions. Our results demonstrate that SIF and PRI responded to heat and drought with different sensitivities and thresholds and can serve as diagnostic tools to assess the influence of moderate to extreme environments on terrestrial ecosystems.

1 | Introduction

In recent years, the impact of climate change on the carbon cycle of terrestrial ecosystems has become more apparent. Heatwaves are among the most severe extreme weather events. They are often defined as periods during which temperatures exceed standard conditions for more than a few days. Notably, frequent occurrences of significant drought and heat stress (including heatwaves) have led to a decreased CO_2 uptake by vegetation (Doughty et al. 2015; van der Woude et al. 2023; Wolf et al. 2016). Plants generally close their stomata under drought conditions (Chaves et al. 2003; Damour et al. 2010), thereby restricting gas exchange and reducing the photosynthetic rate. Stomatal closure and the subsequent decrease in photosynthetic rate are often observed at noon, especially under high temperatures and saturated light conditions; this phenomenon is known as midday depression (MD; Tenhunen et al. 1984). MD has been reported at both single leaf (e.g.,

This is an open access article under the terms of the Creative Commons Attribution License, which permits use, distribution and reproduction in any medium, provided the original work is properly cited.

© 2026 The Author(s). *Ecological Research* published by John Wiley & Sons Australia, Ltd on behalf of The Ecological Society of Japan.

Muraoka et al. 2000) and canopy (e.g., Pingintha et al. 2010) scales. The occurrence of MD is associated with the soil water content (SWC) and stomatal sensitivity to atmospheric dryness, specifically the vapor pressure deficit (VPD), which is linked to water potential within the plant body (Tardieu and Simonneau 1998; Zweifel et al. 2007).

Cold and hot conditions impose lower and upper thresholds for photosynthesis, and the photosynthetic rate exhibits a bell-shaped response to varying temperatures (Hikosaka et al. 2016). Warmer temperatures generally enhance plant photosynthesis; however, extremely high air and leaf temperatures suppress the photosynthetic rate, owing to the temperature dependence of reactions, including the Rubisco and ribulose bisphosphate limitation mechanisms (Sage and Kubien 2007; Kumarathunge et al. 2019). The temperature response of photosynthesis is characterized by two key parameters: the optimum temperature and the critical temperature. The optimum temperature is the temperature at which the photosynthetic rate reaches its maximum, and the critical temperature is the upper temperature threshold above which photosynthesis rapidly declines. The heatwave effect is tightly linked with the upper threshold. Some photosynthesis models require the optimum and critical temperatures as key parameters to predict responses to heat stress under growth conditions (e.g., Cao et al. 2004).

Photochemical reactions are a major component in determining photosynthetic productivity. It involves light absorption and subsequent energy partitioning by photochemistry (P), chlorophyll fluorescence (F), basal thermal dissipation (D), and regulated thermal dissipation as a nonphotochemical quenching (NPQ) at the photosystems of chloroplasts within a leaf (Porcar-Castell et al. 2014; van der Tol et al. 2014). These photosystem energy-partitioning processes are studied at the single-leaf scale and are specifically important for nondestructive measurement of plant physiological functions at the photosystem level. Using the balance of photosystem energy partitioning (i.e., yields of P, F, D, and NPQ), the fraction of P yield can be estimated, which directly contributes to CO_2 assimilation (Genty et al. 1989; Hendrickson et al. 2004; Kramer et al. 2004). Because the D yield is a basal component, F and NPQ yields mainly influence the short-term determination of P yield. NPQ acts as a safety valve on excess energy and is part of a protection process in photosystems. Thus, NPQ yield and P yield are generally negatively correlated. In contrast, F yield and P yield can be positively related (Flexas et al. 2002), with some exceptions discussed later. Recently, Hikosaka and Noda (2019) proposed an empirical leaf-scale model to estimate the P yield contribution using only two of the competing energy-partition fractions: F and NPQ yields. The study demonstrated the use of short-range remote sensing at a few-centimeter scale, including chlorophyll fluorescence and the photochemical reflectance index (PRI), which indicate F and NPQ, respectively. The advantage of remote sensing is the ability to detect signals over large, distant areas. As such, remote sensing incorporating the energy partition processes has been gaining interest.

Solar-induced chlorophyll fluorescence (SIF) is defined as the fluorescence emitted from plant leaves under sunlight, which is distinguished from the leaf-scale F measured under artificial light. To understand large spatial scale variations, SIF is a widely used passive remote sensing indicator for tracking photosynthetic activity across tower and satellite footprints (Gu et al. 2019; Porcar-Castell et al. 2021; Sun et al. 2023). SIF is evaluated using the Fraunhofer lines spectra of sunlight and reflected radiance from vegetation measured by a fine-resolution hyperspectral radiometer. SIFs retrieved from absorption bands O_2A (760 nm wavelength) and O_2B (687 nm wavelength) are the so-called SIF A (far-red SIF) and SIF B (red SIF), respectively. Most studies focus on SIF A because of its strong O_2A absorption and high reflectance at 760 nm. SIF has been observed with spectroradiometers mounted on towers, airborne platforms, and satellites (Mohammed et al. 2019; Van Wittenberghe et al. 2021). Most SIF remote sensing studies confirm a positive relationship between SIF and gross primary production (GPP; Sun et al. 2023). SIF and GPP are the products of light energy input (absorbed photosynthetically active radiation: APAR), thus photosynthetic light use efficiency (LUE) and the canopy-scale fluorescence yield (SIFyield) can be written based on the LUE equation (Monteith 1972) and an analogous expression of the LUE equation for SIF (Guanter et al. 2014; Yang et al. 2015).

$$\mathrm{GPP} = \mathrm{APAR} \times \mathrm{LUE}, \tag{1}$$

$$\mathrm{SIF} = \mathrm{APAR} \times \mathrm{SIFyield}. \tag{2}$$

This relationship is widely accepted as a fundamental explanation linking SIF and GPP (Sun et al. 2023). However, SIF yield can vary depending on physiological changes under stress or physical factors such as vegetation structure or observation geometry. Recently, reflectance-to-fluorescence theory was developed to scale the signal from the canopy to the leaf, enabling distinction between physiological and physical responses (Yang and van der Tol 2018; Yang et al. 2025; Zeng et al. 2019). Based on this, the canopy fluorescence emission efficiency (εF) was evaluated.

$$\mathrm{SIFyield} = \varepsilon F \times f_{\mathrm{esc}}, \tag{3}$$

where f_{esc} is the fraction of fluorescence escaping from the canopy. The fraction depends on scattering and absorption, which affect the physical variations of SIF. The advantage of retrieving εF is that it can be scaled to one of the components of the photosystem energy partition (as F yield) in the canopy. There is generally a positive relationship, albeit with wide variations, between LUE and εF (Kim et al. 2021; Wieneke et al. 2018; Yang et al. 2015).

The PRI is a remote sensing indicator of NPQ (Gamon et al. 1997; Hikosaka and Noda 2019; Nakaji et al. 2006). PRI is estimated from spectral reflectance differences at wavelengths of 531 and 570 nm caused by variations in xanthophyll pigments. Based on the negative (competing) relationship between LUE and NPQ yield, PRI can be used to estimate LUE from leaf measurement (Porcar-Castell et al. 2012), flux tower footprint remote sensing (Gamon 2015; Nakaji et al. 2014), and drone remote sensing (D'Odorico et al. 2021).

The assumption of a monotonic response between stress factors and indicators, such as SIF and PRI, ignores thresholds and competing processes. Recent findings have expressed concern regarding oversimplification in its applications. Several studies on grasslands, croplands, and mixed land covers in rural

TABLE 1 | Hypothetical scenarios of indicators' responses to heatwave conditions.

		Scenario A	Scenario B	Scenario C
Indicator variables	**Target variables**	**Extreme heat–drought**	**Drought-triggered**	**Heat-triggered**
εF	F-yield	V-shape (turning point)	Moderate	↓ Late
ΔPRI	NPQ-yield	Saturated	↓ Early	↓ Early
Additional explanatory		Simultaneous change-point of two variables	Coupling of g_s–VPD	Abrupt threshold

Abbreviations: ↓, decline of variables; g_s, stomatal conductance; NPQ, non-photochemical quenching; VPD, vapor pressure deficit; ΔPRI, photochemical reflectance index corrected by dark state values; εF, canopy fluorescence emission efficiency.

areas have shown that satellite SIF (e.g., Kiyono et al. 2023; Sun et al. 2015; Yoshida et al. 2015) and εF (e.g., Kimm et al. 2021) have been applied as indicators of plant response to environmental stresses such as drought and heatwave. However, the applicability of SIF or εF depends on the specific thresholds used. For example, high-light intensity and stress conditions tend to produce a reversed response with increasing εF and declining P yield (Magney et al. 2020). Indeed, the relationship between εF and LUE shifts from positive to negative under extreme heat–drought conditions because saturating NPQ alters the dissipation pathway (Martini et al. 2022). This alternation is simply explained by the fact that F- and P-yield compete within the pathways if the safety valve (i.e., NPQ) does not function. However, the precise determination of the saturating NPQ remains questionable, and the closure of stomata and enhanced heat-related fluorescence emission over 40°C have been proposed as possible alternative explanations (Antala et al. 2025). As such, information on NPQ, stomata, and temperature ranges is key to clarifying the εF variations during heatwaves. The NPQ contributions can be evaluated under heat–drought stress using PRI (Nakaji et al. 2006; Ide et al. 2010). However, PRI depends on reflectance changes caused by pigment variation or measurement angle geometry, and it may introduce biases when scaling NPQ across the canopy (Biriukova et al. 2020). Despite these limitations, measurements of εF and PRI may provide evidence of energy partitioning and serve as a diagnostic for ranges and types of stresses. Here, potential scenarios were proposed based on previous findings, assuming that εF and PRI successfully indicate F- and NPQ-yield (Table 1). In scenario A, extreme heat and drought alter the energy pathway, and εF passes the turning point and increases with higher stress when PRI is saturated (e.g., Martini et al. 2022). In scenario B, mediated drought triggers a rapid PRI response and a gradual εF response, with a significant correlation between stomatal conductance and VPD (e.g., Flexas et al. 2002). In scenario C, extreme heat stress triggers PRI decline, followed by a sharp drop once the NPQ threshold (e.g., ~35°C) is exceeded, and εF declines moderately and slowly until higher thresholds (e.g., Haldimann and Feller 2004).

In the present study, we focused on an extreme high-temperature and high-air-dryness event, defined here as a short heatwave (StHW), recorded in the inland areas of the Japanese mainland in July–early August 2022. Evaluating the stress response of trees to extreme events in the forest ecosystem will improve the ability to monitor environmental change. The aims of this study were as follows: (1) to demonstrate MD in sub-hourly GPP and SIF during the StHW and pre-heatwave periods; (2) to assess the temperature dependency of GPP and SIF in relation to the optimum temperature; and (3) to examine εF–PRI response scenarios A, B, and C above and identify drivers of remote sensing indicators from moderate to extreme conditions in a larch forest.

2 | Materials and Methods

2.1 | Study Site

The study was conducted in a cool-temperate deciduous needle-leaved coniferous forest at the northern foot of Mt. Fuji, at Fujihokuroku (FHK; N35.443°, E138.765°)—one of the Asiaflux sites. The CO_2 flux has been measured with eddy covariance methods since 2003. The altitude and mean slope of the site are 1100 m a.s.l. and 3°, respectively. The forest consists of a 60-year-old plantation of Japanese larch (*Larix kaempferi* (Lamb.) Carrière), established during the national land afforestation campaign in the 1950s during the Showa era, which is typical of mountain land-use history in Japan. The understory is dominated by ferns (*Dryopteris crassirhizoma* Nakai), deciduous shrubs including cherry bushes (*Cerasus incisa* (Thunb.) Loisel. var. *incisa*), and herbaceous plant species. Because the forest is a plantation, there is a homogeneous vegetation cover over an area of 1 km × 1 km. The stem density was 249 ha^{-1}, and the basal area was 27.1 $m^2 ha^{-1}$ in 2016 (Teramoto et al. 2019). The canopy tree height was approximately 25 m. The leaf area index (LAI) values of the overstory and understory were approximately 3.1 and 2.4 (leaf area/ground area, m^2 m^{-2}), respectively (Akitsu et al. 2020). Mean annual temperature and precipitation were 8.9°C and 1831 mm between 2006 and 2023 (AsiaFlux 2025). The near-surface soil is covered by Holocene volcanic scoria. The soil has high porosity and high water permeability, and it is categorized as the hydrological percolating zone of the mountain (Yamamoto 1970). Forest thinning treatment was conducted in 2014–2015 (Teramoto et al. 2019), with no artificial disturbance thereafter.

2.2 | Identification of the 2022 Short Heatwave

The meteorological extreme was assessed from 18 years of daily maximum air temperature and VPD in a half-hourly observation dataset from 2006 to 2024 from the FHK tower site. The 90th and 10th percentiles were defined as the upper and lower thresholds of climatology. Using criteria similar to those in Hobday et al. (2016), a StHW, which is also called a heat spike, was detected from 30 July to 3 August 2022 (days of the year: DOY 211–215), exceeding the upper threshold at close to a Ta

of 27°C or VPD of 17 hPa (Figure 1). The early part of the StHW (DOY > 214) was relatively close to the upper threshold, and the latter part (DOY 214–215) reflected a more extreme heat–drought condition. By contrast, there was no clear SWC extreme in late July to August (Figure A1). The Annual Regional Meteorological Report mentioned the record high temperature was due to a Pacific high-pressure system (JMA 2023).

2.3 | Tower Spectroscopy and Remote Sensing Indices

A 3-fiber optics-2-spectrometer system (Morozumi et al. 2024) was installed at the 32-m tower to measure SIF above the forest canopy (Figure 2). A red/far-red region fluorescence spectrometer (QEpro, Ocean Insight, FL, USA; range 650–800 nm; interval 0.15 nm; full-width half max 0.3 nm) and a wide visible near-infrared spectrometer (Flame-S, Ocean Insight, range 350–1000 nm; spectral sampling interval 0.3 nm; full-width half max 1.3 nm) were installed to observe SIF and other vegetation indices. Optical fibers measured three signals (Figure 2), of which we used two: (i) downwelling hemispherical incident solar irradiance with a cosine corrector (CC-3, Ocean Insight) and (ii) a directional upwelling radiance for vegetation with bare fiber (FOV 25°) with view zenith angle at 45° and view azimuth angle at 0° (looking northward) to capture the sunlit leaf signals effectively near noon. The view-angle dependency of SIF warrants technical consideration, as discussed in Morozumi et al. (2023). Thus, the third signal (iii), the nadir-hemispherical aperture, was not used to simplify the findings in this study. Each fiber channel was controlled by mechanical shutters (TTL-s, Ocean Insight), which were switched in sequence within a 1-min interval at the beginning of each 5-min interval. The individual spectral shape is shown in Figure 2a,b. Canopy-scale SIF was retrieved from atmospheric

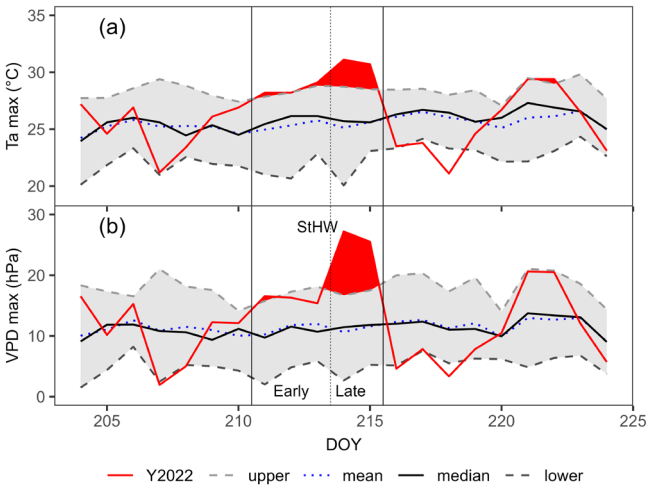


FIGURE 1 | Extreme event recorded from the daily mean air temperature at the study site from 30 July to 3 August 2022 (filled with red). (a) The mean and median of daily maximum air temperature (Ta max) and (b) vapor pressure deficit (VPD max) among 18-year data at the flux tower are plotted (dotted blue and solid gray) with upper and lower 90th percentile thresholds (dashed gray lines). The days of the year (DOY) in 211–215 were the short heatwave period (StHW; with vertical solid lines) separated into the early (DOY < 214) and late periods (DOY ≥ 214; vertical dotted line).

oxygen absorption bands (O_2 A: 760 nm) using the improved Fraunhofer Line Discrimination (iFLD; Julitta et al. 2016), with the 750–780 nm region, based on the incident and outgoing radiation as follows:

$$L_{veg} = R\frac{E_{sun}}{\pi} + \mathrm{SIF}, \tag{4}$$

where L_{veg} is outgoing radiance from vegetation, R is vegetation reflectance, E_{sun} is incident solar irradiance, and SIF is fluorescence radiance from vegetation.

The iFLD method was selected for its reliability in generating an hourly-scale SIF signal (Kukkurainen et al. 2025). Output stability was tested among different retrievals, including the band shape-fitting method (van der Tol et al. 2023) and the 3FLD method, and between different instruments (Figures S1 and S2).

To extract the physiological information without light-dependent variations in the canopy-level SIF O_2A signal, the canopy fluorescence emission efficiency εF was calculated using the radiation and the fluorescence correction vegetation index (FCVI: Yang et al. 2020) as follows:

$$\varepsilon F = \frac{\pi \mathrm{SIF}}{\mathrm{PAR} \times \mathrm{FCVI}}, \tag{5}$$

where photosynthetic active radiation (PAR) was defined at 400–700 nm wavelength above the canopy, and FCVI was calculated from the reflectance of two bands in the near-infrared (R_{NIR}: 770 nm) and the visible band (R_{VIS}: 400–700 nm).

$$\mathrm{FCVI} = R_{NIR} - R_{VIS}. \tag{6}$$

To estimate physiological information of the NPQ response to stress factors, the PRI was calculated from reflectance at 531 and 570 nm using Equation (7) (Gamon et al. 1997):

$$\mathrm{PRI} = \frac{R_{531} - R_{570}}{R_{531} + R_{570}}. \tag{7}$$

PRI can be influenced by canopy structure and the relative density of chlorophyll and xanthophyll pigments, and the index should be corrected to estimate NPQ using dark-state PRI_0 values as the reference baseline (Gamon and Berry 2012). To correct for this baseline variation, delta PRI (ΔPRI) was defined as the difference between the instantaneous PRI and the dark-state PRI (PRI_0). In this study, PRI_0 was evaluated on each day from the maximum PRI value among early morning (6:00–8:00) and late afternoon (16:00–18:00). The equation for ΔPRI follows:

$$\Delta\,\mathrm{PRI} = \mathrm{PRI} - \mathrm{PRI}_0. \tag{8}$$

2.4 | Eddy Covariance CO_2/H_2O Flux Measurements

The CO_2 and H_2O fluxes were measured at the tower facility using an anemometer-thermometer (CSAT-3, Campbell Scientific, UT, USA), a closed-path analyzer (LI-7000, LI-Cor, Lincoln, NE, USA), and an open-path analyzer (LI-7500, LI-Cor). Air temperature, relative humidity, and precipitation were measured using a probe (HMP155D, Vaisala, Helsinki, Finland) and a rain gauge (CYG-52202, R. M. Yong, MI, USA) at the top

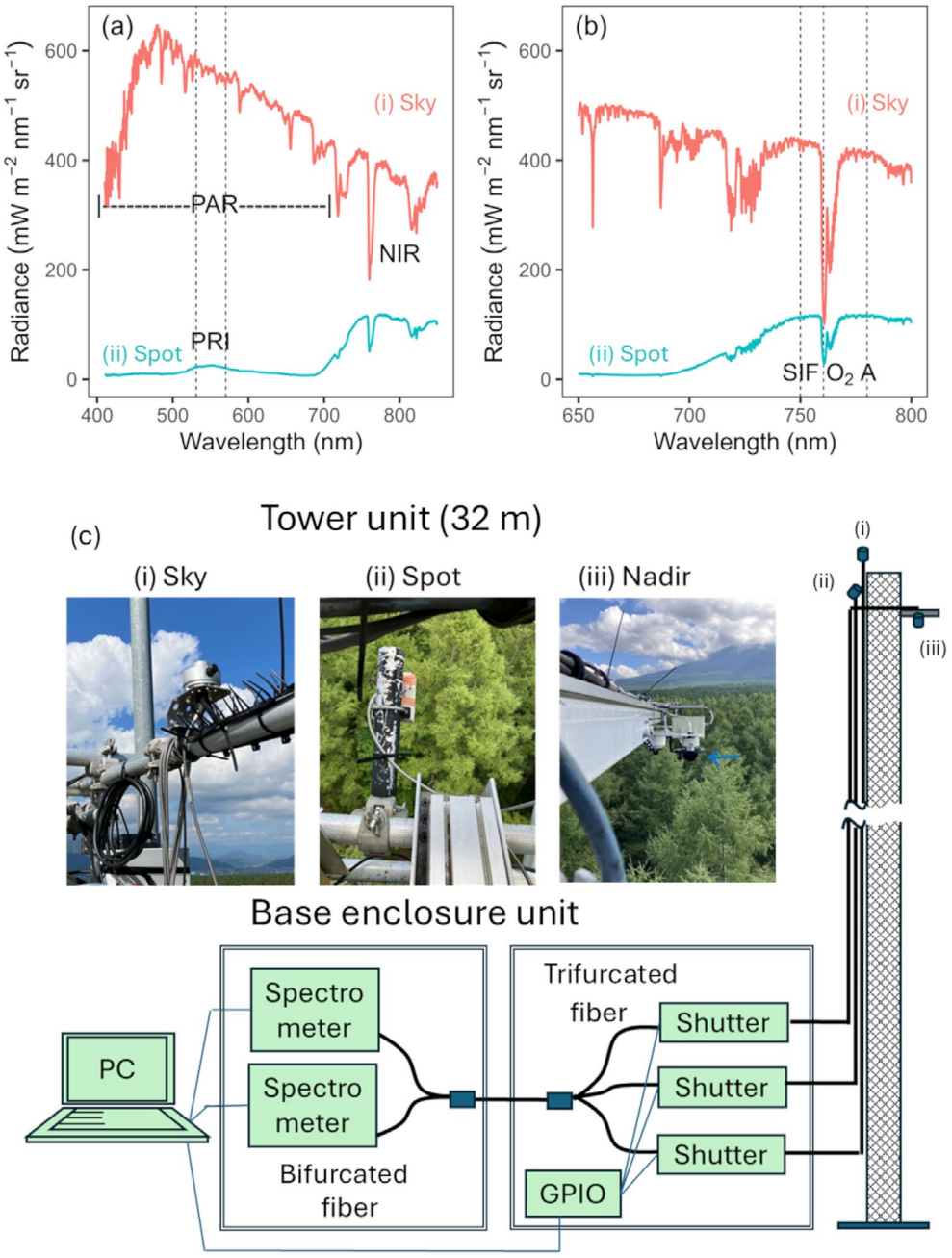


FIGURE 2 | Spectral radiance data in (a) a wide-range spectrometer, (b) a narrow-range fluorescence detection spectrometer. Legends of (a) and (b): Red and blue indicate incident sunlight (i: Sky) and outgoing radiance from vegetation (ii: Spot). The vertical dashed line and horizontal line indicate the specific wavelength to evaluate SIF, NIR, PRI, and PAR. NIR, near-infrared radiance. (c) Spectral measurement systems consist of tower units mounted on the aluminum tower facility and a base enclosure unit set in the field laboratory. Foreoptics on tower units are capturing (i) sky, (ii) spotting to the larch tree crowns, and (iii) the nadir vegetation signal. Shutters open one by one to ensure that the sky or vegetation signals enter the inlet of the spectrometers separately. PAR, photosynthetic active radiation; PRI, photochemical reflectance index; SIF O_2A, solar induced chlorophyll fluorescence in oxygen-A band.

of the tower (32 m). Photosynthetically active photon flux density was measured by quantum sensors (LI-190S, LI-Cor; SQ-110, Apogee USA) to evaluate PAR. Absorbed PAR within the canopy (APAR) was calculated from four sensors ($APAR = \downarrow PAR_{32m} - \uparrow PAR_{30m} - \downarrow PAR_{2m} + \uparrow PAR_{2m}$; with arrows indicating the upward↑ or downward↓ directions of radiation in the forest). In three replicates, SWC was measured as a volumetric water content unit by time-domain reflectometers (CS616, Campbell Scientific) below ground (0.1 and 0.2 m). Fluxes of sensible heat (H, W m^{-2}), latent heat (LE, W m^{-2}), and CO_2 (Fc, μmol m^{-2} s^{-1}) were calculated for 30-min intervals using the eddy covariance method. Finally, GPP and ecosystem respiration were obtained from daily and nocturnal variations in net ecosystem exchange, calculated from Fc and a storage term based on CO_2 concentration measurements. Evapotranspiration (ET, mm h^{-1}) was converted from LE with the latent heat of vaporization. For details of the flux and meteorological measurements, see Takahashi et al. (2015). The LUE of photosynthesis (mol CO_2

mol^{-1} photons) was calculated at the canopy scale from the ratio of instantaneous GPP and absorbed PAR (=GPP/APAR).

We analyzed the canopy conductance (g_s) as a characteristic of canopy-scale stomata responses to water and environmental factors (Takanashi et al. 2010). The surface conductance of water vapor (g_s, mm s^{-1}) was calculated on the basis of the Penman–Monteith equation (Monteith 1965), implemented by algorithms in the *bigleaf* package (Knauer et al. 2018) in R software (R Core Team 2022), using Equation (9):

$$g_s = \frac{LEr_a\gamma}{\Delta\left(R_n - G - S\right) + \rho c_p r_a D_a - LE(\Delta + \gamma)}, \quad (9)$$

where Rn is the net radiation (W m^{-2}), G is the ground heat flux (W m^{-2}), S is the vegetation heat storage (W m^{-2}), Da is the dew point, r_a is the aerodynamic conductance to heat transfer calculated with the wind speed and the friction velocity, ρ is the air density, c_p is the heat capacity, Δ is the slope of the saturation vapor pressure curve, and γ is the psychrometric constant (kPa K^{-1}).

2.5 | Statistical Analysis

The statistical analysis was computed using the R software v4.2.2 (R Core Team 2022). Remote sensing variables were quality-checked for incident light stability between two spectrometers within 25% and reflectance stability within 0.2–0.9 at 750 nm, and then averaged to a half-hourly mean. The statistics were analyzed after filtering rainfall (> 0.1 mm) to avoid unintended errors in optics caused by light rain, dew, and overpassing clouds.

Temperature dependency was assessed for SIF, GPP, and g_s with a quadratic equation (e.g., Kumarathunge et al. 2019), as follows:

$$A = A_{\text{opt}} - b\left(Ta - T_{\text{opt}}\right)^2, \quad (10)$$

where A_{opt} is the value of the dependent variable in optimal temperature, Ta is air temperature, b is the curvature coefficient, and T_{opt} is the optimum temperature.

To minimize the light-dependent variances, data were filtered by daytime (8:00–16:00) and APAR > 900 μmol m^{-2}s^{-1}, assuming the relative light saturation when MD was obviously observed in diurnal variations. The non-linear least-squares regression method was applied to fit equation (10) using mean values binned into 1°C intervals. The variable dependencies for εF, ΔPRI, and LUE were assessed with piecewise regression (Toms and Lesperance 2003) to depict the ecological threshold. The scatter plots were analyzed according to the fit to the above non-linear models and linear regression models. Pearson's correlation coefficient r and p-values between estimates and input variables were evaluated. Local weighted smoothing was also applied to scatter plots on the diurnal cycle. To summarize the statistical significance between two paired variables, a t-test was performed. The time window for the paired category was defined as 9:00–15:00 in the main results. However, other combinations of time windows were tested across 6:00–19:00 (Figure S3). The one-way bootstrap ANOVA (*WRS2* package in R; Mair et al. 2025) was applied to test the statistical significance of variables across three timepoint categories (Before heatwave, Early heatwave, and Late heatwave) because it is robust to non-normality and to smaller sample sizes.

3 | Results

GPP, SIF, APAR, and other meteorological variables showed diurnal and daily variations during DOY 204–224, 2022 (Figure 3), although the patterns of change differed. During the study period, major rainfall was observed (> 5 mm day^{-1}) on DOY 207, 216, and 224, and SWC (> 21 vol%) was relatively high on DOY 208 and 217 (Figure A1). After rainfall, VPD tended to show a gradual increase while SWC decreased. Thus, the datasets contained three sets of wet–dry gradients through StHW and non-StHW periods. The sky condition was mostly sunny except on DOY 212 when APAR was < 500 (μmol m^{-2}s^{-1}), during the StHW. Other variables, including LUE, ΔPRI, εF, and gs, also varied with Ta (17.9°C–31°C), VPD (0–27.1 hPa), and SWC (18.3–23.4 vol%). The scatter points on each day indicate sub-daily variations from 6:00 to 18:00.

The diurnal variations in APAR, VPD, and SIF shown in Figure 4 clarify the difference in the diurnal patterns during the early and late parts of the StHW (DOY 211–215) and before the heatwave period under the clear sky (DOY 205–206). Half-hourly GPP and SIF varied from 10.8 to 44.3 (μmol CO_2 m^{-2}s^{-1}) and 0.0466–1.25 (mW m^{-2}nm^{-1}sr^{-1}) within a daytime period lasting 6:00–18:00, and there was a day-to-day difference, especially from noon to afternoon (Figure 4c,d). Extremely high air temperatures (26.5°C–31°C) and VPD (9.7–27.1 hPa) led to a significant decline in SIF and GPP (28% and 16%, respectively) during the daytime (9:00–15:00) when comparing pre-StHW, early-StHW, and late-StHW (Figure 3e–h). The diurnal course of GPP reached its maximum in the morning and then declined until noon in late-StHW. Thus, the larch forest experienced an MD of photosynthesis activity.

We showed the relationships between GPP, SIF, and air temperature in the half-hourly intervals during daytime (8:00–16:00) under high incident radiation (APAR > 900) during the study period, including the StHW (Figure 5). The optimum temperature for GPP (21.7°C) was higher than that for SIF at 26.8°C. εF declined gradually with increasing temperature, with an optimum at 23.8°C (Figure A2). The g_s also declined with temperature (Figure 5c) and VPD (Figure A3), and there was no peak for g_s among the observed conditions (Ta ≥ 21°C; Figure A3).

Each of the relationships between meteorological factors and the variables εF, ΔPRI, and LUE differed (Figure 6, Table 2). Among the meteorological factors, VPD had substantial linear negative effects (Figure 6a–c), where statistics were $r = -0.29$ ($p < 0.0001$), $r = -0.71$ ($p < 0.0001$), and $r = -0.59$ ($p < 0.0001$) for εF, ΔPRI, and LUE. The breakpoint in the LUE–VPD relationship was clear and relatively saturated (no significance) at VPD > 12 hPa (Figure 6c). The ΔPRI and LUE showed a similar pattern with responses to VPD. The influences of Ta were similar to VPD, but patterns of breakpoints and segmented piecewise linear regressions were more diverse among variables (Figure 6d–f). There was a lower correlation with LUE ($r = -0.55$) in Ta than with that in VPD. The correlation coefficients of εF remained moderate, with or without breakpoints. Notably, there was a clear breakpoint near an SWC of 21%, and εF and SWC showed a significant positive correlation only in drier conditions (Figure 6g). ΔPRI–SWC and LUE–SWC

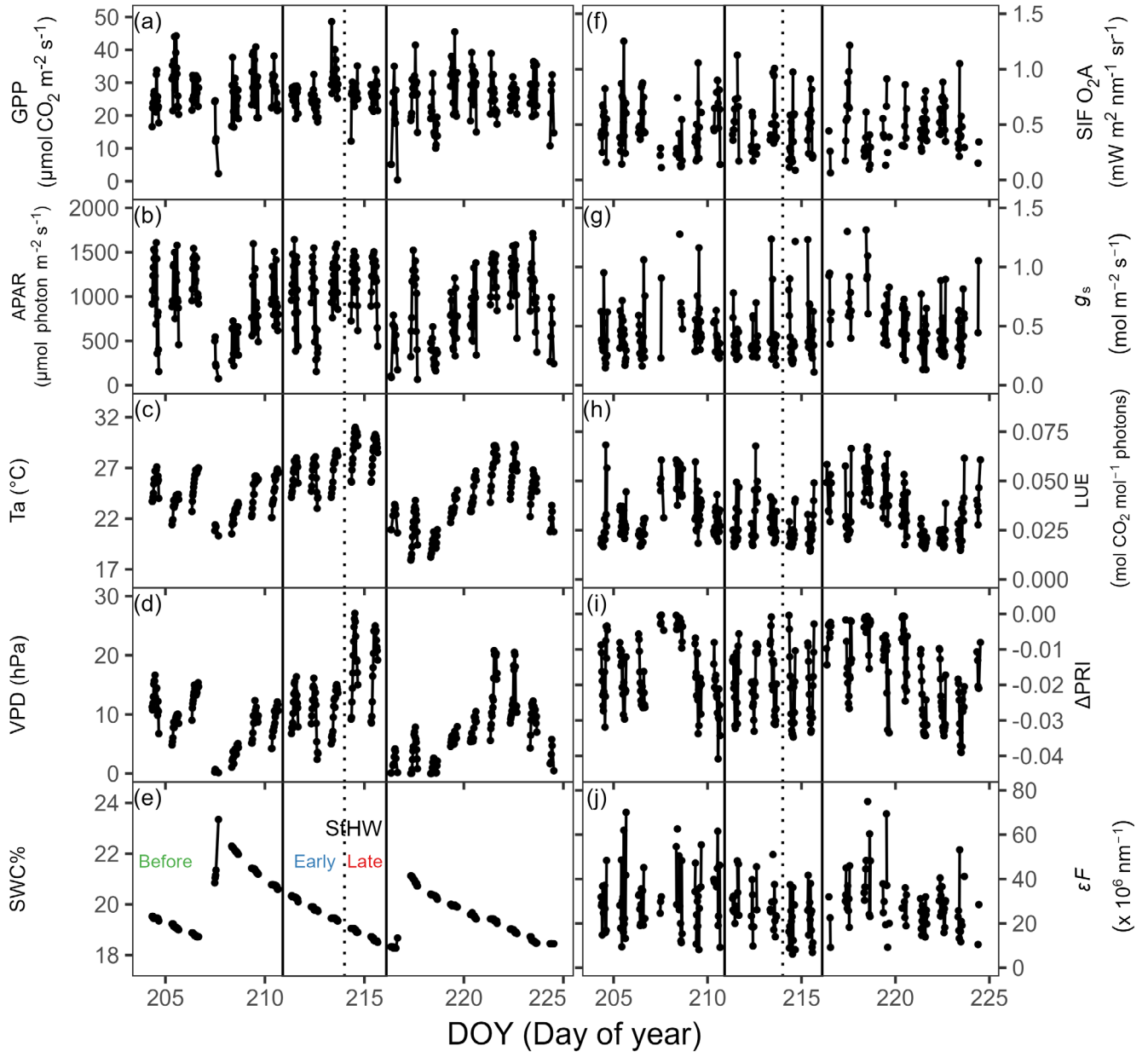


FIGURE 3 | Temporal variations for (a) GPP, (b) APAR, (c) Ta, (d) VPD, (e) SWC, (f) SIF, (g) g_s, (h) LUE, (i) ΔPRI, and (j) εF, on a half-hourly scale (8:00–16:00) during late July–early August (days of the year DOY: 204–224). Vertical solid lines indicate the start and the end of the short heatwave period (StHW). The dotted line indicates the boundary between the early and late periods of the StHW. The beginning of the target period (DOY 205–206; sunny conditions) is categorized as "before StHW" as a reference in Figure 4. ΔPRI, delta photochemical reflectance index corrected by dark state values; APAR, absorbed photosynthetically active radiation; GPP, Gross primary productivity; g_s, canopy conductance; LUE, light use efficiency; SIF, solar-induced chlorophyll fluorescence; SWC, soil water content; Ta, air temperature; VPD, vapor pressure deficit; εF, canopy fluorescence emission efficiency.

were similarly positive, but correlation coefficients remained weak at $r < 0.2$ in drier conditions (Figure 6h–i).

4 | Discussion

4.1 | The Extreme Heat Surpassed the Optimum Temperature of SIF and GPP

In the present study, we demonstrated the effect of the extreme heat on diurnal SIF and GPP. There were temperature thresholds (22°C–27°C) at which GPP and SIF reached maximum values. Beyond those thresholds, when conditions were too warm, values declined. Thus, it appeared that the optimum temperature for photosynthetic activity and fluorescence emissions was surpassed in the deciduous needle-leaved larch forest. The optimum temperature of various biomes has been reported using flux observation (Chang et al. 2021; Niu et al. 2012), although there are few records for deciduous needle-leaf forest. Thus, the study provides a unique larch forest dataset that is currently missing. Previous studies have demonstrated the optimum temperature for photosynthesis in juvenile planted larch trees. Values include 21.8°C–23.8°C in Hokkaido, northern Japan (Harayama

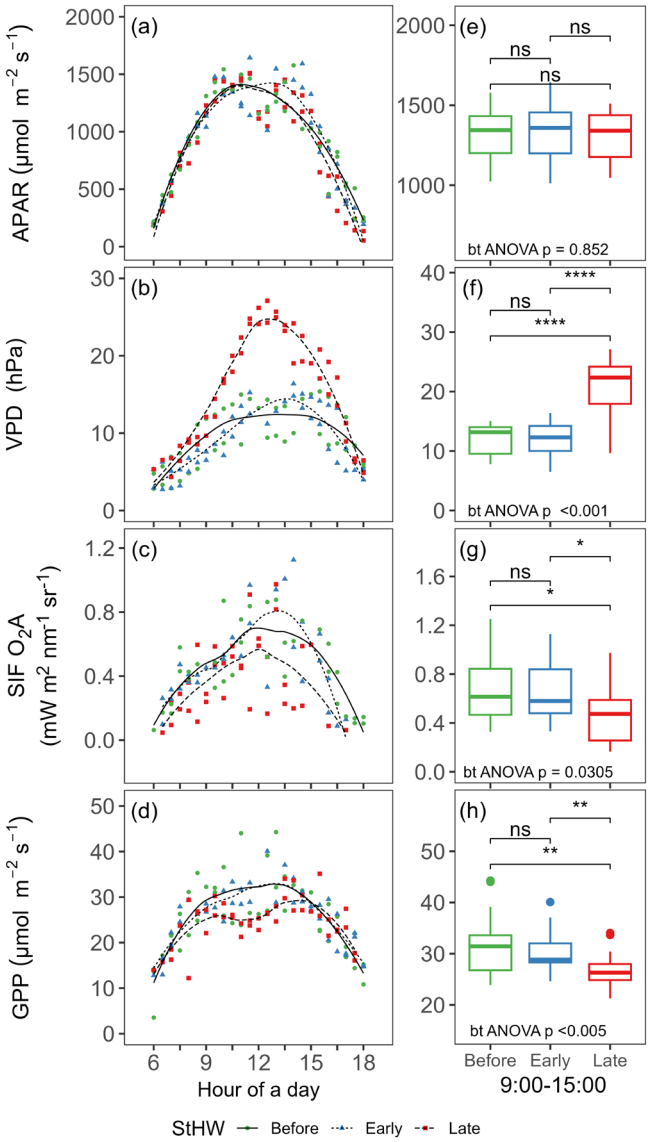


FIGURE 4 | Half-hourly variation of (a) APAR, (b) VPD, (c) SIF, and (d) GPP on days of the year (DOY) 205–206 (before heatwave: Green dots with solid line), DOY 211–213 (Early: Blue triangles with dotted line), and DOY 214–215 (Late: Red dots with dashed line). Box car plots for variables (e–h) among three periods (Before, Early, and Late in the StHW). Stars indicate statistical significance (****$p < 0.0001$, **$p < 0.01$, *$p < 0.05$) and bottom p-values indicate significance of the bootstrap ANOVA. APAR, absorbed photosynthetically active radiation; bt ANOVA, bootstrap analysis of variance; GPP, gross primary productivity; SIF, solar-induced chlorophyll fluorescence; StHW, short heatwave period; VPD, vapor pressure deficit.

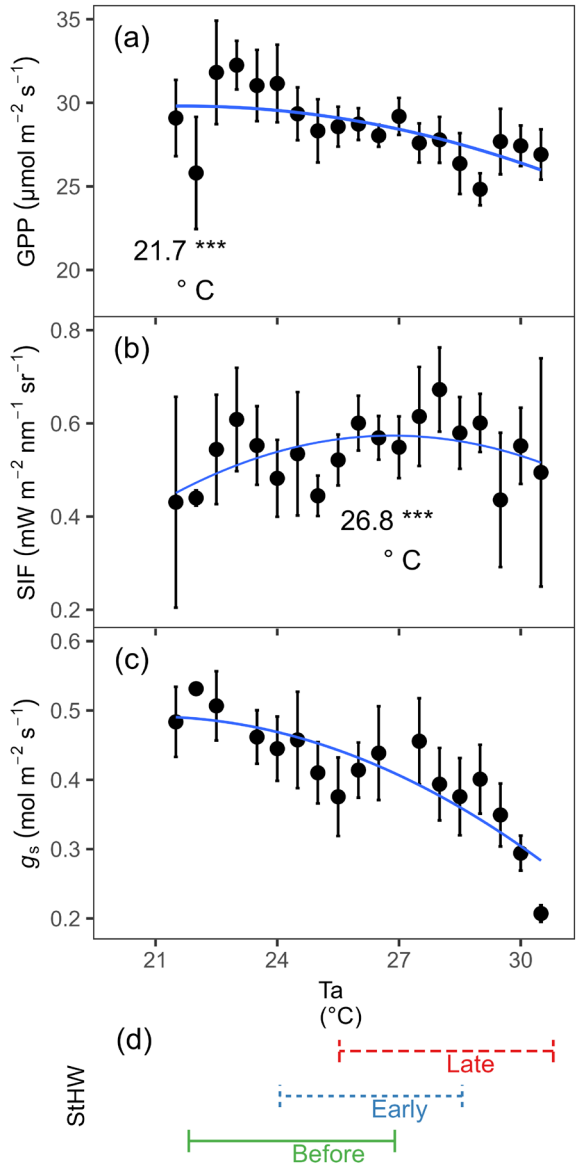


FIGURE 5 | The relationship between air temperature and (a) GPP, (b) SIF, and (c) g_s during the study period, days of the year (DOY) 204–224 (including before and after the heatwave period). Fitted lines indicate quadratic regressions with optimal temperatures. Stars indicate statistical significance (***$p < 0.001$, *$p < 0.1$). (d) The bottom color lines indicate the air temperature range in three periods (Before, Early, and Late in the StHW). GPP, gross primary productivity; g_s, canopy conductance; SIF, solar-induced chlorophyll fluorescence; StHW, short heatwave.

et al. 2012); 22.5°C–25°C in northeast China (Ju et al. 2022); 18°C–23°C (Higgins et al. 1987) and 15°C–21°C (Crane Jr. et al. 1983) in northern North America. Our findings are within the range of these larch samples. In other tree species in the cool-temperate region of Japan, the optimum temperature was estimated to be much higher, 25°C–29°C, for *Quercus crispula* Blume (Hikosaka et al. 2007).

It should be noted that the optimum temperature for SIF was much higher than that for GPP. That difference was supported by the canopy-scale efficiency-based variables—εF showed higher optima than those for LUE. This likely reflects the difference in the temperature dependencies of fluorescence emission and CO_2-concentration-related modulation at the Rubisco reaction rate (Greer 2022). Thus, under heat stress, SIF may reflect the safety margin of the temperature limit known as the critical temperature (discussed in Section 4.3).

4.2 | Air and Soil Drought Stress on Photosynthesis and Its Proxies

We also demonstrated that, among environmental factors such as air temperature and soil dryness, VPD had the most

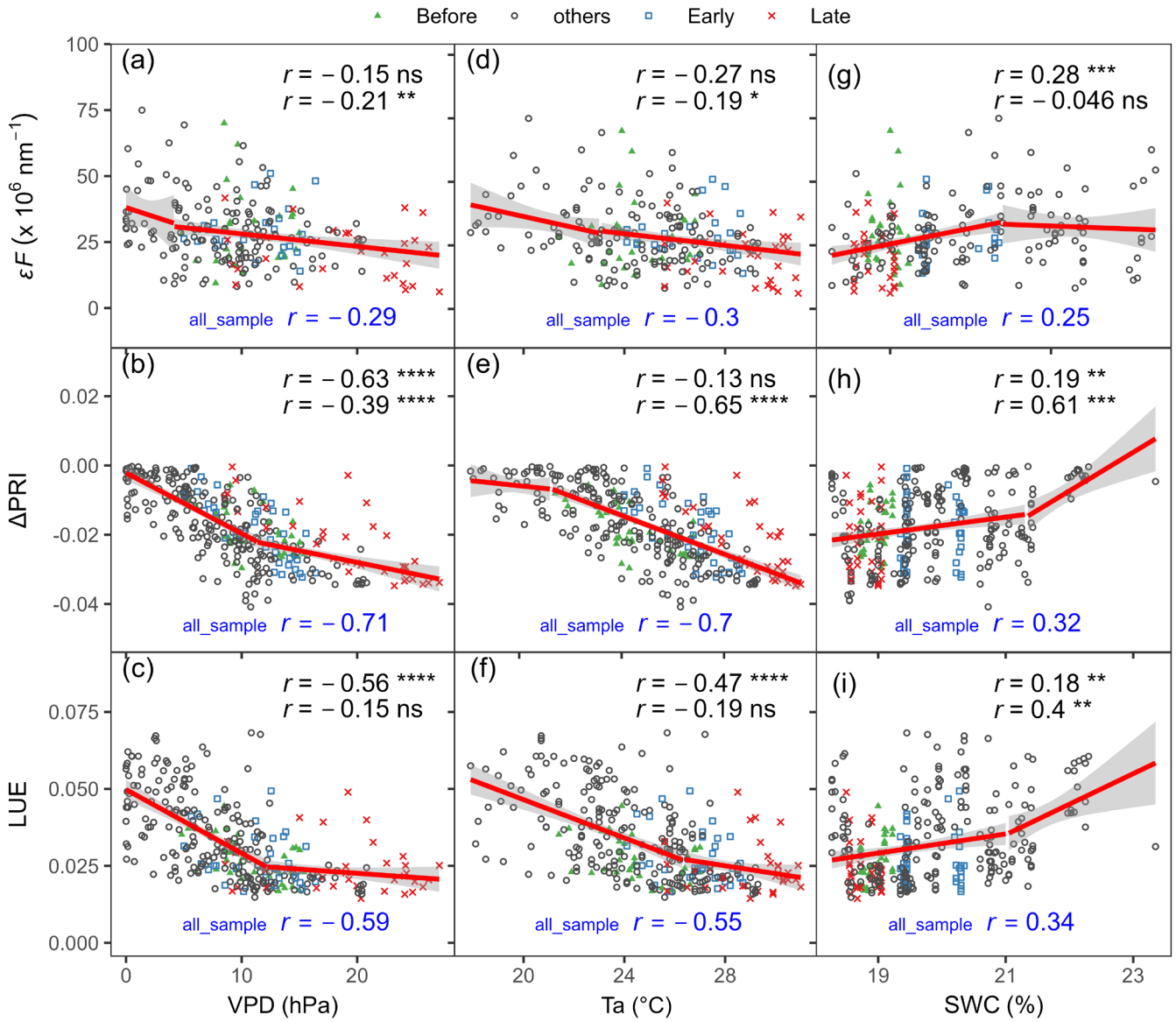


FIGURE 6 | The relationships between vegetation variables (εF, ΔPRI, and LUE) and environmental factors (VPD, SWC, and Ta). Subplots include (a) εF–VPD, (b) ΔPRI–VPD, (c) LUE–VPD, (d) εF–Ta, (e) ΔPRI–Ta, (f) LUE–Ta, (g) εF–SWC, (h) ΔPRI–SWC, and (i) LUE–SWC. Red lines with gray shaded areas indicate piecewise linear regressions and standard errors. The correlation coefficient r across all scatter points is at the bottom in purple, and r for piecewise regressions is at the upper right in black, where the upper r indicates the correlation coefficient of lower x-values and vice versa. The asterisks indicate statistical significance (****$p < 0.0001$, ***$p < 0.001$, **$p < 0.01$, *$p < 0.05$, ns, not significant). The correlation coefficients for all samples are significant ($p < 0.001$ or $p < 0.0001$) in every subplot (a–i), and asterisks are not shown. The legend colors indicate three key periods (Before, Early, and Late StHW, as in Figure 4), and the other complementary days include after StHW (others). ΔPRI, delta photochemical reflectance index corrected by dark state values; LUE, light use efficiency; StHW, short heatwave; SWC, soil water content; Ta, air temperature; VPD, vapor pressure deficit; εF, canopy fluorescence emission efficiency.

TABLE 2 | Summary of responses among the indicator and environmental explanatory variables from the results in Figure 5.

Indicator variables	Target variables	Air dryness (VPD) responses	Air temperature (Ta) responses	Soil dryness responses
εF	F-yield	Moderate	Moderate	↓ Low SWC
ΔPRI	NPQ-yield	↓ Early	↓ Late	Moderate
LUE	P-yield	↓ Early (saturated at higher)	↓ Early (saturated at higher)	Moderate

Abbreviations: ↓, decline of variables; LUE, light use efficiency; NPQ, non-photochemical quenching; SWC, soil water content; Ta, air temperature; VPD, vapor pressure deficit; ΔPRI, photochemical reflectance index corrected by dark state values; εF, canopy fluorescence emission efficiency.

substantial impact on photosynthetic decline, likely through its influence on stomatal closure (see Figure S4, which shows actual stomatal distribution in a larch needle). The result clearly refuted scenario A: reversed (v-shaped) F-yield with simultaneous NPQ saturation and altered energy partitioning (Tables 1 and 2) and supported scenario B (drought response with coupling of stomatal regulation) as a reasonable explanation. This finding is consistent with a previous study by Xu et al. (2020), which showed that stomatal responses were the most significant factor affecting GPP during heatwave events at several flux sites in the mid-latitudes. In Siberian boreal forests, high stomatal conductance and no clear MD were reported for larch (Maximov et al. 2019). However, Nakaji et al. (2006) found that MD was observed on a shoot of a mature larch tree in northern Japan. A warmer climate might be a possible explanation for the findings. The study on a mature larch also demonstrated the sensitivity of ΔPRI to heat/drought because ΔPRI was strongly correlated with Ta and VPD (Nakaji et al. 2006). The relationship between ΔPRI and stress factors suggests that thermal dissipation was enhanced via an increasing fraction of NPQ under stress. The stomatal responses to VPD were well fitted to a simple regression line, with a steeper slope at < 10 hPa and then reaching saturation (Figure A3). This finding was similar to a previous study for *Larix decidua* Mill. (Leo et al. 2014), in which anisohydric behaviors were reported. Conifer trees are typically reported as having isohydric characteristics that sustain the water potential with stomatal behavior, although such isohydric/anisohydric characteristics are not bipolar in actual data (Schumann et al. 2024). One limitation of the current study is that it lacks sap flow data or leaf water potential supporting the physical limit of water stress (e.g., cavitation).

The relationship between VPD and εF supported the consistent sensitivity of SIF to stress factors even during the heatwave period. A suppressed SIF or εF with high VPD has been reported in several tower-based observation studies in deciduous broadleaf forest, mixed forest, and croplands (e.g., Cheng et al. 2022; Morozumi et al. 2023; Paul-Limoges et al. 2018; Yi et al. 2024), and a consistent positive correlation between SIF and GPP is well established under stressed conditions. However, contrasting findings were reported in evergreen *Quercus ilex* woodland (Martini et al. 2022), in *Populus deltoides* Bartr. ex Marshall (Helm et al. 2020) and in *Liriodendron tulipifera* L., *Quercus palustris* Münchh. and *Quercus alba* L. (Marrs et al. 2020). These findings conflict with the accepted concept of photosynthesis–drought responses tracked through a steady-state fluorescence signal (Flexas et al. 2002), which is theoretically the same as leaf-level SIF. Different regulation mechanisms for high temperature and drought/water limitation can result in complex responses. Such differences may derive from species-specific strategies for water limitation (e.g., the relative plasticity of the transpiration function on *Larix decidua* trees; Peters et al. 2019). Thus, considering the effect of plant functional types and severity conditions of heat and water would improve the deterministic model using SIF and εF. For this purpose, a geographical dataset on water-stress-resistant strategies for mature trees could serve as a possible input. Another proxy of stomatal activity can be assessed using carbonyl sulfide (Lai et al. 2024), which may also help constrain the explanation of SIF variation. A scenario-based interpretation and further investigation of the threshold range are also necessary, especially to distinguish between heat- and drought-related effects on SIF.

SWC also had a critical influence on εF, although its effect was not clearly reflected in LUE or PRI in this study. This suggests that εF, which responded more moderately than PRI to rapid air dryness change, remains more sensitive to plant water-limited stress under low water availability. Satellite SIF, combined with SWC, revealed a sharp decline in SIF under dry conditions in Mongolia (Kiyono et al. 2023) and US regions (Short Gianotti et al. 2019). The thresholds of rapid fluorescence declines, as shown in previous studies, were 15%–21% SWC. Liu et al. (2020) further demonstrated that the impact of soil moisture was more significant than that of VPD on the spatial variation of global SIF data. As such, our results support the expectation that fluorescence remote sensing can be used in the study of plant–water relationships.

4.3 | Regional Aspects of High-Temperature Environments and Future Research

It is important to monitor the regional impact of heat–drought-related events. The recorded heat–drought event in 2022 was climatologically extreme or anomalous (Figure 1). This extreme was not limited to the local impact on the Mt. Fuji area but was a part of the record-breaking high temperature in Japan from late June to July (JMA 2023) and of heatwaves across the Eurasian continent in 2022 (Wang et al. 2023). Against such a background, we need to consider regional impacts. The thermal tipping point (i.e., critical temperature), a more severe temperature threshold compared with the thermal optimum, is the proxy of temperatures where photosynthesis is disrupted, and chloroplasts are damaged irreversibly (Marchin et al. 2022). The climate model simulation for Mongolia's boreal larch forest predicted a potential surpassing of the thermal tipping point in 2050 (Rao et al. 2023). As a part of a general trend, larch growing at a much lower latitude, like in Japan and northeastern China (Takagi et al. 2015), would also often surpass optimum temperatures and face critical temperatures in the future. Extreme high temperatures are predicted to cause more protein-related downregulation, such as photosystem damage, rather than stomatal-related downregulation in photosynthesis (e.g., Marchin et al. 2022; Mathur et al. 2014; Sato et al. 2024). Therefore, future studies should clarify these metabolic response scenarios, including the optimal conditions and thresholds in warming environments. The next challenge may involve explicitly assessing the canopy-scale photosystem energy partitioning through hourly indicators such as SIF, PRI, and other leaf-level measurements. Remote sensing of vegetation physiology, such as SIF, combined with the site-scale evaluation like this study, will help to understand large-scale drought–heat responses. Multiscale insights into ecosystem responses can be synthesized for adaptation or mitigation under climate change.

5 | Conclusions

We presented a stress-response assessment of tower CO_2 flux and remote sensing of PRI and SIF during a short-term extreme

heatwave in a cool-temperate *Larix kaempferi* forest. The findings demonstrated a significant decline in GPP and SIF at noon in the latter half of the heatwave period when the VPD was extremely high. The optimum temperatures for SIF and GPP were surpassed during the heatwave. Notably, the optimum temperature for SIF was apparently higher than that for GPP, and thus the potential application of the critical temperature threshold was discussed using SIF. We tested the three response pattern scenarios under extreme conditions, assuming co-occurring altered photosystem energy partition, drought-triggering, and heat-triggering responses, using efficiency-based indicators, and found that drought was the most reasonable case. ΔPRI and LUE were substantially affected by the VPD and air temperature, followed by a moderate εF sensitivity. The analysis of canopy conductance supported the drought-related stomatal responses and suggested plant functional differences in resistance to heatwaves. Our results suggest that the rapid ΔPRI response to drought may decline and nearly reach saturation earlier than εF, and that SIF and scaled chlorophyll fluorescence indicators may help extend the ecological indicator's role under future extremes. The scenario-based approaches for interpreting remote sensing indicators demonstrated by this study can be usefully applied to assessing ecosystem response to environmental changes.

Acknowledgments

The authors would like to thank Dr. Nyein Chan (Kyoto University of Advanced Science *at present*) and Dr. Tomoki Kiyono (Yokohama National University *at present*) from the Satellite Observation Center and the staff who contributed to the FHK Station including Dr. Ryuichi Hirata and Dr. Reiko Ide, Center for Global Environmental Research in the National Institute for Environmental Studies, for their cooperation with this study. We would like to acknowledge Dr. Tomoko Akitsu's kind cooperation on the LAI data. We thank Edanz (https://jp.edanz.com/ac) for editing a draft of this manuscript.

Funding

This research was funded by the program for NIES-SYKE (the Finnish Environmental Institute) collaborative research activities and the Strategic Research Program "Climate Change and Air Quality Research Program" of National Institute for Environmental Studies (NIES) and Environment Research and Technology Development Fund (JPMEERF20193003; 2-1903) of the Environmental Restoration and Conservation Agency of Japan (ERCA) and the KAKENHI program (JP21K17873, JP24H01525) of the Japan Society for the Promotion of Science (JSPS).

Conflicts of Interest

Dr. Tomomichi Kato is one of the Editorial Board members of *Ecological Research*, but he had no involvement in the peer review and decision-making processes for this paper.

Data Availability Statement

The remote sensing data of the presented study are available from the Global Environmental Database (GED) via National Institute for Environmental Studies, Japan (https://doi.org/10.17595/20260512.001). The flux data are accessible via the AsiaFlux database (https://db.cger.nies.go.jp/asiafluxdb/). The LAI data are accessible via the Japan Long-term Terrestrial Ecological Research JaLTER database (http://db.cger.nies.go.jp/JaLTER/metacat/metacat/ERDP-2020-16.1/jalter-en) and the updated URL will be available (https://doi.org/10.1111/1440-1703.70035).

References

Akitsu, T. K., T. Nakaji, H. Kobayashi, et al. 2020. "Large-Scale Ecological Field Data for Satellite Validation in Deciduous Forests and Grasslands." *Ecological Research* 35, no. 6: 1009–1028. https://doi.org/10.1111/1440-1703.12155.

Antala, M., R. Juszczak, and A. Rastogi. 2025. "Nonphotochemical Quenching Does Not Alter the Relationship Between Sun-Induced Fluorescence and Gross Primary Production Under Heatwave." *New Phytologist* 245, no. 3: 927–930. https://doi.org/10.1111/nph.20312.

AsiaFlux HP. 2025. https://asiaflux.net/index.php?page_id=54.

Biriukova, K., M. Celesti, A. Evdokimov, et al. 2020. "Effects of Varying Solar-View Geometry and Canopy Structure on Solar-Induced Chlorophyll Fluorescence and PRI." *International Journal of Applied Earth Observation and Geoinformation* 89: 102069. https://doi.org/10.1016/j.jag.2020.102069.

Cao, M., S. D. Prince, J. Small, and S. J. Goetz. 2004. "Remotely Sensed Interannual Variations and Trends in Terrestrial Net Primary Productivity 1981–2000." *Ecosystems* 7, no. 3: 233–242. https://doi.org/10.1007/s10021-003-0189-x.

Chang, Q., X. Xiao, R. Doughty, X. Wu, W. Jiao, and Y. Qin. 2021. "Assessing Variability of Optimum Air Temperature for Photosynthesis Across Site-Years, Sites and Biomes and Their Effects on Photosynthesis Estimation." *Agricultural and Forest Meteorology* 298–299: 108277. https://doi.org/10.1016/j.agrformet.2020.108277.

Chaves, M., J. Maroco, and J. Pereira. 2003. "Understanding Plant Responses to Drought—From Genes to the Whole Plant." *Functional Plant Biology* 30, no. 3: 239–264. https://doi.org/10.1071/FP02076.

Cheng, X., M. Hu, Y. Zhou, et al. 2022. "The Divergence of Micrometeorology Sensitivity Leads to Changes in GPP/SIF Between Cork Oak and Poplar." *Agricultural and Forest Meteorology* 326: 109189. https://doi.org/10.1016/j.agrformet.2022.109189.

Crane, J. L., Jr., D. I. Dickmann, and J. A. Flore. 1983. "Photosynthesis and Transpiration by Young *Larix kaempferi* Trees: C3 Responses to Light and Temperature." *Physiologia Plantarum* 59, no. 4: 635–640. https://doi.org/10.1111/j.1399-3054.1983.tb06292.x.

Damour, G., T. Simonneau, H. Cochard, and L. Urban. 2010. "An Overview of Models of Stomatal Conductance at the Leaf Level." *Plant, Cell & Environment* 33: 1419–1438. https://doi.org/10.1111/j.1365-3040.2010.02181.x.

D'Odorico, P., L. Schönbeck, V. Vitali, et al. 2021. "Drone-Based Physiological Index Reveals Long-Term Acclimation and Drought Stress Responses in Trees." *Plant, Cell & Environment* 44, no. 11: 3552–3570. https://doi.org/10.1111/pce.14177.

Doughty, C. E., D. B. Metcalfe, C. A. J. Girardin, et al. 2015. "Drought Impact on Forest Carbon Dynamics and Fluxes in Amazonia." *Nature* 519, no. 7541: 78–82. https://doi.org/10.1038/nature14213.

Flexas, J., J. M. Escalona, S. Evain, et al. 2002. "Steady-State Chlorophyll Fluorescence (Fs) Measurements as a Tool to Follow Variations of Net CO_2 Assimilation and Stomatal Conductance During Water-Stress in C3 Plants." *Physiologia Plantarum* 114, no. 2: 231–240. https://doi.org/10.1034/j.1399-3054.2002.1140209.x.

Gamon, J. A. 2015. "Reviews and Syntheses: Optical Sampling of the Flux Tower Footprint." *Biogeosciences* 12, no. 14: 4509–4523. https://doi.org/10.5194/bg-12-4509-2015.

Gamon, J. A., and J. A. Berry. 2012. "Facultative and Constitutive Pigment Effects on the Photochemical Reflectance Index (PRI) in Sun and Shade Conifer Needles." *Israel Journal of Plant Sciences* 60, no. 1–2: 85–95. https://doi.org/10.1560/IJPS.60.1-2.85.

Gamon, J. A., L. Serrano, and J. S. Surfus. 1997. "The Photochemical Reflectance Index: An Optical Indicator of Photosynthetic Radiation

Use Efficiency Across Species, Functional Types, and Nutrient Levels." *Oecologia* 112, no. 4: 492–501. https://doi.org/10.1007/s004420050337.

Genty, B., J.-M. Briantais, and N. R. Baker. 1989. "The Relationship Between the Quantum Yield of Photosynthetic Electron Transport and Quenching of Chlorophyll Fluorescence." *Biochimica et Biophysica Acta (BBA) - General Subjects* 990, no. 1: 87–92. https://doi.org/10.1016/S0304-4165(89)80016-9.

Greer, D. H. 2022. "Leaf Temperature and CO_2 Effects on Photosynthetic CO_2 Assimilation and Chlorophyll a Fluorescence Light Responses During Mid-Ripening of *Vitis vinifera* cv. Shiraz Grapevines Grown in Outdoor Conditions." *Functional Plant Biology* 49, no. 7: 659–671.

Gu, L. H., J. M. Han, J. D. Wood, C. Y. Y. Chang, and Y. Sun. 2019. "Sun-Induced Chl Fluorescence and Its Importance for Biophysical Modeling of Photosynthesis Based on Light Reactions." *New Phytologist* 223, no. 3: 1179–1191. https://doi.org/10.1111/nph.15796.

Guanter, L., Y. G. Zhang, M. Jung, et al. 2014. "Global and Time-Resolved Monitoring of Crop Photosynthesis With Chlorophyll Fluorescence." *Proceedings of the National Academy of Sciences of the United States of America* 111: E1327–E1333. https://doi.org/10.1073/pnas.1320008111.

Haldimann, P., and U. Feller. 2004. "Inhibition of Photosynthesis by High Temperature in Oak (*Quercus pubescens* L.) Leaves Grown Under Natural Conditions Closely Correlates With a Reversible Heat-Dependent Reduction of the Activation State of Ribulose-1,5-Bisphosphate Carboxylase/Oxygenase." *Plant, Cell & Environment* 27, no. 9: 1169–1183. https://doi.org/10.1111/j.1365-3040.2004.01222.x.

Harayama, H., A. Uemura, S. Kitaoka, H. Utsugi, Y. Ono, and K. Kita. 2012. "Temperature and Vapor Pressure Deficit Dependence of Photosynthetic Rate in Saplings of Three *Larix* spp." *Boreal Forest Research (Hoppo Shinrin Kenkyu)* 60: 29–30. https://doi.org/10.24494/jfsh.60.0_29.

Helm, L. T., H. Shi, M. T. Lerdau, and X. Yang. 2020. "Solar-Induced Chlorophyll Fluorescence and Short-Term Photosynthetic Response to Drought." *Ecological Applications* 30, no. 5: e02101. https://doi.org/10.1002/eap.2101.

Hendrickson, L., R. T. Furbank, and W. S. Chow. 2004. "A Simple Alternative Approach to Assessing the Fate of Absorbed Light Energy Using Chlorophyll Fluorescence." *Photosynthesis Research* 82, no. 1: 73–81. https://doi.org/10.1023/B:PRES.0000040446.87305.f4.

Higgins, S. S., R. A. Black, G. K. Radamaker, and W. R. Bidlake. 1987. "Gas Exchange Characteristics and Water Relations of Larixoccidentalis." *Canadian Journal of Forest Research* 17, no. 11: 1364–1370. https://doi.org/10.1139/x87-211.

Hikosaka, K., E. Nabeshima, and T. Hiura. 2007. "Seasonal Changes in the Temperature Response of Photosynthesis in Canopy Leaves of Quercus Crispula in a Cool-Temperate Forest." *Tree Physiology* 27, no. 7: 1035–1041. https://doi.org/10.1093/treephys/27.7.1035.

Hikosaka, K., and H. M. Noda. 2019. "Modeling Leaf CO_2 Assimilation and Photosystem II Photochemistry From Chlorophyll Fluorescence and the Photochemical Reflectance Index." *Plant, Cell & Environment* 42, no. 2: 730–739. https://doi.org/10.1111/pce.13461.

Hikosaka, K., K. Noguchi, and I. Terashima. 2016. "Modeling Leaf Gas Exchange." In *Canopy Photosynthesis: From Basics to Applications*, edited by K. Hikosaka, Ü. Niinemets, and N. P. R. Anten, 61–100. Springer. https://doi.org/10.1007/978-94-017-7291-4_3.

Hobday, A. J., L. V. Alexander, S. E. Perkins, et al. 2016. "A Hierarchical Approach to Defining Marine Heatwaves." *Progress in Oceanography* 141: 227–238. https://doi.org/10.1016/j.pocean.2015.12.014.

Ide, R., T. Nakaji, and H. Oguma. 2010. "Assessment of Canopy Photosynthetic Capacity and Estimation of GPP by Using Spectral Vegetation Indices and the Light–Response Function in a Larch Forest." *Agricultural and Forest Meteorology* 150, no. 3: 389–398. https://doi.org/10.1016/j.agrformet.2009.12.009.

JMA. 2023. *Climate Change Monitoring Report 2022*. Japan Meteorological Association.

Ju, Y., C. Wang, N. Wang, and X. Quan. 2022. "Transplanting Larch Trees Into Warmer Areas Increases the Photosynthesis and Its Temperature Sensitivity." *Tree Physiology* 42, no. 12: 2521–2533. https://doi.org/10.1093/treephys/tpac084.

Julitta, T., M. Migliavacca, and T. Wutzler. 2016. "FieldSpectroscopy CC and FieldSpectroscopy DP Packages." *Online on GitHub Platform*. https://github.com/tommasojulitta/FieldSpectroscopyDP.

Kim, J., Y. Ryu, B. Dechant, et al. 2021. "Solar-Induced Chlorophyll Fluorescence Is Non-Linearly Related to Canopy Photosynthesis in a Temperate Evergreen Needleleaf Forest During the Fall Transition." *Remote Sensing of Environment* 258: 112362. https://doi.org/10.1016/j.rse.2021.112362.

Kimm, H., K. Guan, C. Jiang, et al. 2021. "A Physiological Signal Derived From Sun-Induced Chlorophyll Fluorescence Quantifies Crop Physiological Response to Environmental Stresses in the U.S. Corn Belt." *Environmental Research Letters* 16, no. 12: 124051. https://doi.org/10.1088/1748-9326/ac3b16.

Kiyono, T., H. M. Noda, T. Kumagai, et al. 2023. "Regional-Scale Wilting Point Estimation Using Satellite SIF, Radiative-Transfer Inversion, and Soil-Vegetation-Atmosphere Transfer Simulation: A Grassland Study. Journal of Geophysical Research." *Biogeosciences* 128, no. 4: e2022JG007074. https://doi.org/10.1029/2022JG007074.

Knauer, J., T. S. El-Madany, S. Zaehle, and M. Migliavacca. 2018. "Bigleaf—An R Package for the Calculation of Physical and Physiological Ecosystem Properties From Eddy Covariance Data." *PLoS One* 13, no. 8: e0201114. https://doi.org/10.1371/journal.pone.0201114.

Kramer, D. M., G. Johnson, O. Kiirats, and G. E. Edwards. 2004. "New Fluorescence Parameters for the Determination of QA Redox State and Excitation Energy Fluxes." *Photosynthesis Research* 79, no. 2: 209–218. https://doi.org/10.1023/B:PRES.0000015391.99477.0d.

Kukkurainen, A., A. Lipponen, V. Kolehmainen, A. Arola, S. Cogliati, and N. Sabater. 2025. "SIFFI: Bayesian Solar-Induced Fluorescence Retrieval Algorithm for Remote Sensing of Vegetation." *Remote Sensing of Environment* 318: 114558. https://doi.org/10.1016/j.rse.2024.114558.

Kumarathunge, D. P., B. E. Medlyn, J. E. Drake, et al. 2019. "Acclimation and Adaptation Components of the Temperature Dependence of Plant Photosynthesis at the Global Scale." *New Phytologist* 222, no. 2: 768–784. https://doi.org/10.1111/nph.15668.

Lai, J., L. M. J. Kooijmans, W. Sun, et al. 2024. "Terrestrial Photosynthesis Inferred From Plant Carbonyl Sulfide Uptake." *Nature* 634: 855–861. https://doi.org/10.1038/s41586-024-08050-3.

Leo, M., W. Oberhuber, R. Schuster, T. E. E. Grams, R. Matyssek, and G. Wieser. 2014. "Evaluating the Effect of Plant Water Availability on Inner Alpine Coniferous Trees Based on Sap Flow Measurements." *European Journal of Forest Research* 133, no. 4: 691–698. https://doi.org/10.1007/s10342-013-0697-y.

Liu, L., L. Gudmundsson, M. Hauser, D. Qin, S. Li, and S. I. Seneviratne. 2020. "Soil Moisture Dominates Dryness Stress on Ecosystem Production Globally." *Nature Communications* 11, no. 1: 4892. https://doi.org/10.1038/s41467-020-18631-1.

Lohammar, T., S. Larsson, S. Linder, and S. Falk. 1980. "FAST: Simulation Models of Gaseous Exchange in Scots Pine." *Ecological Bulletins* 32: 505–523.

Magney, T. S., M. L. Barnes, and X. Yang. 2020. "On the Covariation of Chlorophyll Fluorescence and Photosynthesis Across Scales." *Geophysical Research Letters* 47, no. 23: e2020GL091098. https://doi.org/10.1029/2020GL091098.

Mair, P., R. Wilcox, and I. Patil. 2025. "A Collection of Robust Statistical Methods (WRS2) Version 1.1–7." https://doi.org/10.32614/CRAN.package.WRS2.

Marchin, R. M., D. Backes, A. Ossola, M. R. Leishman, M. G. Tjoelker, and D. S. Ellsworth. 2022. "Extreme Heat Increases Stomatal Conductance and Drought-Induced Mortality Risk in Vulnerable Plant Species." *Global Change Biology* 28, no. 3: 1133–1146. https://doi.org/10.1111/gcb.15976.

Marrs, J. K., J. S. Reblin, B. A. Logan, et al. 2020. "Solar-Induced Fluorescence Does Not Track Photosynthetic Carbon Assimilation Following Induced Stomatal Closure." *Geophysical Research Letters* 47, no. 15: e2020GL087956. https://doi.org/10.1029/2020GL087956.

Martini, D., K. Sakowska, G. Wohlfahrt, et al. 2022. "Heatwave Breaks Down the Linearity Between Sun-Induced Fluorescence and Gross Primary Production." *New Phytologist* 233, no. 6: 2415–2428. https://doi.org/10.1111/nph.17920.

Mathur, S., D. Agrawal, and A. Jajoo. 2014. "Photosynthesis: Response to High Temperature Stress." *Stress and Photosynthesis* 137: 116–126. https://doi.org/10.1016/j.jphotobiol.2014.01.010.

Maximov, T. C., A. P. Maksimov, A. V. Kononov, A. Kotani, and A. J. Dolman. 2019. "Carbon Cycles in Forests." In *Water-Carbon Dynamics in Eastern Siberia*, edited by T. Ohta, T. Hiyama, Y. Iijima, A. Kotani, and T. C. Maximov, 69–100. Springer Singapore. https://doi.org/10.1007/978-981-13-6317-7_4.

Mohammed, G. H., R. Colombo, E. M. Middleton, et al. 2019. "Remote Sensing of Solar-Induced Chlorophyll Fluorescence (SIF) in Vegetation: 50 Years of Progress." *Remote Sensing of Environment* 231: 39. https://doi.org/10.1016/j.rse.2019.04.030.

Monteith, J. L. 1965. "Evaporation and Environment." *Society for Experimental Biology* 19: 205–234.

Monteith, J. L. 1972. "Solar Radiation and Productivity in Tropical Ecosystems." *Journal of Applied Ecology* 9: 747–766. https://doi.org/10.2307/2401901.

Morozumi, T., T. Kato, H. Kobayashi, et al. 2023. "Row Orientation Influences the Diurnal Cycle of Solar-Induced Chlorophyll Fluorescence Emission From Wheat Canopy, as Demonstrated by Radiative Transfer Modeling." *Agricultural and Forest Meteorology* 339: 109576. https://doi.org/10.1016/j.agrformet.2023.109576.

Morozumi, T., T. Kato, H. Kobayashi, H. Noda, and T. Matsunaga. 2024. "Ground-Based Spectral Measurements of Solar-Induced Chlorophyll Fluorescence for Validation of GOSAT-GW TANSO-3." *Journal of the Remote Sensing Society of Japan* 44, no. 2: 170–176. https://doi.org/10.11440/rssj.2024.005.

Muraoka, H., Y. Tang, I. Terashima, H. Koizumi, and I. Washitani. 2000. "Contributions of Diffusional Limitation, Photoinhibition and Photorespiration to Midday Depression of Photosynthesis in *Arisaema heterophyllum* in Natural High Light." *Plant, Cell & Environment* 23, no. 3: 235–250. https://doi.org/10.1046/j.1365-3040.2000.00547.x.

Nakaji, T., Y. Kosugi, S. Takanashi, et al. 2014. "Estimation of Light-Use Efficiency Through a Combinational Use of the Photochemical Reflectance Index and Vapor Pressure Deficit in an Evergreen Tropical Rainforest at Pasoh, Peninsular Malaysia." *Remote Sensing of Environment* 150: 82–92. https://doi.org/10.1016/j.rse.2014.04.021.

Nakaji, T., H. Oguma, and Y. Fujinuma. 2006. "Seasonal Changes in the Relationship Between Photochemical Reflectance Index and Photosynthetic Light Use Efficiency of Japanese Larch Needles." *International Journal of Remote Sensing* 27, no. 3: 493–509. https://doi.org/10.1080/01431160500329528.

Niu, S., Y. Luo, S. Fei, et al. 2012. "Thermal Optimality of Net Ecosystem Exchange of Carbon Dioxide and Underlying Mechanisms." *New Phytologist* 194, no. 3: 775–783.

Paul-Limoges, E., A. Damm, A. Hueni, et al. 2018. "Effect of Environmental Conditions on Sun-Induced Fluorescence in a Mixed Forest and a Cropland." *Remote Sensing of Environment* 219: 310–323. https://doi.org/10.1016/j.rse.2018.10.018.

Peters, R. L., M. Speich, C. Pappas, et al. 2019. "Contrasting Stomatal Sensitivity to Temperature and Soil Drought in Mature Alpine Conifers." *Plant, Cell & Environment* 42, no. 5: 1674–1689. https://doi.org/10.1111/pce.13500.

Pingintha, N., M. Y. Leclerc, J. P. Beasley Jr., et al. 2010. "Hysteresis Response of Daytime Net Ecosystem Exchange During Drought." *Biogeosciences* 7, no. 3: 1159–1170. https://doi.org/10.5194/bg-7-1159-2010.

Porcar-Castell, A., J. I. Garcia-Plazaola, C. J. Nichol, et al. 2012. "Physiology of the Seasonal Relationship Between the Photochemical Reflectance Index and Photosynthetic Light Use Efficiency." *Oecologia* 170: 313–323. https://doi.org/10.1007/s00442-012-2317-9.

Porcar-Castell, A., Z. Malenovský, T. Magney, et al. 2021. "Chlorophyll a Fluorescence Illuminates a Path Connecting Plant Molecular Biology to Earth-System Science." *Nature Plants* 7, no. 8: 998–1009.

Porcar-Castell, A., E. Tyystjarvi, J. Atherton, et al. 2014. "Linking Chlorophyll a Fluorescence to Photosynthesis for Remote Sensing Applications: Mechanisms and Challenges." *Journal of Experimental Botany* 65, no. 15: 4065–4095. https://doi.org/10.1093/jxb/eru191.

R Core Team. 2022. "R: A Language and Environment for Statistical Computing." R Foundation for Statistical Computing (Version 4.2.2) [Software].

Rao, M. P., N. K. Davi, T. S. Magney, et al. 2023. "Approaching a Thermal Tipping Point in the Eurasian Boreal Forest at Its Southern Margin." *Communications Earth & Environment* 4, no. 1: 247. https://doi.org/10.1038/s43247-023-00910-6.

Sage, R. F., and D. S. Kubien. 2007. "The Temperature Response of C3 and C4 Photosynthesis." *Plant, Cell & Environment* 30, no. 9: 1086–1106. https://doi.org/10.1111/j.1365-3040.2007.01682.x.

Sato, H., J. Mizoi, K. Shinozaki, and K. Yamaguchi-Shinozaki. 2024. "Complex Plant Responses to Drought and Heat Stress Under Climate Change." *Plant Journal* 117, no. 6: 1873–1892. https://doi.org/10.1111/tpj.16612.

Schumann, K., B. Schuldt, M. Fischer, C. Ammer, and C. Leuschner. 2024. "Xylem Safety in Relation to the Stringency of Plant Water Potential Regulation of European Beech, Norway Spruce, and Douglas-Fir Trees During Severe Drought." *Trees* 38, no. 3: 607–623. https://doi.org/10.1007/s00468-024-02499-5.

Short Gianotti, D. J., A. J. Rigden, G. D. Salvucci, and D. Entekhabi. 2019. "Satellite and Station Observations Demonstrate Water Availability's Effect on Continental-Scale Evaporative and Photosynthetic Land Surface Dynamics." *Water Resources Research* 55, no. 1: 540–554. https://doi.org/10.1029/2018WR023726.

Sun, Y., R. Fu, R. Dickinson, et al. 2015. "Drought Onset Mechanisms Revealed by Satellite Solar-Induced Chlorophyll Fluorescence: Insights From Two Contrasting Extreme Events." *Journal of Geophysical Research: Biogeosciences* 120, no. 11: 2427–2440. https://doi.org/10.1002/2015JG003150.

Sun, Y., L. Gu, J. Wen, et al. 2023. "From Remotely Sensed Solar-Induced Chlorophyll Fluorescence to Ecosystem Structure, Function, and Service: Part I—Harnessing Theory." *Global Change Biology* 29, no. 11: 2926–2952. https://doi.org/10.1111/gcb.16634.

Takagi, K., R. Hirata, I. Ryuichi, et al. 2015. "Spatial and Seasonal Variations of CO_2 Flux and Photosynthetic and Respiratory Parameters of Larch Forests in East Asia." *Soil Science and Plant Nutrition* 61, no. 1: 61–75. https://doi.org/10.1080/00380768.2014.990349.

Takahashi, Y., N. Saigusa, R. Hirata, et al. 2015. "Characteristics of Temporal Variations in Ecosystem CO_2 Exchange in a Temperate Deciduous Needle-Leaf Forest in the Foothills of a High Mountain." *Journal of Agricultural Meteorology* 71, no. 4: 302–317. https://doi.org/10.2480/agrmet.D-14-00009.

Takanashi, S., Y. Kosugi, S. Ohkubo, N. Matsuo, M. Tani, and A. R. Nik. 2010. "Water and Heat Fluxes Above a Lowland Dipterocarp Forest in Peninsular Malaysia." *Hydrological Processes: An International Journal* 24, no. 4: 472–480.

Tardieu, F., and T. Simonneau. 1998. "Variability Among Species of Stomatal Control Under Fluctuating Soil Water Status and Evaporative Demand: Modelling Isohydric and Anisohydric Behaviours." *Journal of Experimental Botany* 49, no. Special_Issue: 419–432. https://doi.org/10.1093/jxb/49.Special_Issue.419.

Tenhunen, J. D., O. L. Lange, J. Gebel, W. Beyschlag, and J. A. Weber. 1984. "Changes in Photosynthetic Capacity, Carboxylation Efficiency, and CO_2 Compensation Point Associated With Midday Stomatal Closure and Midday Depression of Net CO_2 Exchange of Leaves of *Quercus suber*." *Planta* 162, no. 3: 193–203. https://doi.org/10.1007/BF00397440.

Teramoto, M., N. Liang, Y. Takahashi, et al. 2019. "Enhanced Understory Carbon Flux Components and Robustness of Net CO_2 Exchange After Thinning in a Larch Forest in Central Japan." *Agricultural and Forest Meteorology* 274: 106–117. https://doi.org/10.1016/j.agrformet.2019.04.008.

Toms, J. D., and M. L. Lesperance. 2003. "Piecewise Regression: A Tool for Identifying Ecological Thresholds." *Ecology* 84, no. 8: 2034–2041. https://doi.org/10.1890/02-047.

van der Tol, C., J. A. Berry, P. K. E. Campbell, and U. Rascher. 2014. "Models of Fluorescence and Photosynthesis for Interpreting Measurements of Solar-Induced Chlorophyll Fluorescence." *Journal of Geophysical Research – Biogeosciences* 119, no. 12: 12. https://doi.org/10.1002/2014jg002713.

van der Tol, C., T. Julitta, P. Yang, et al. 2023. "Retrieval of Chlorophyll Fluorescence From a Large Distance Using Oxygen Absorption Bands." *Remote Sensing of Environment* 284: 113304. https://doi.org/10.1016/j.rse.2022.113304.

van der Woude, A. M., W. Peters, E. Joetzjer, et al. 2023. "Temperature Extremes of 2022 Reduced Carbon Uptake by Forests in Europe." *Nature Communications* 14, no. 1: 6218. https://doi.org/10.1038/s41467-023-41851-0.

Van Wittenberghe, S., N. Sabater, M. P. Cendrero-Mateo, et al. 2021. "Towards the Quantitative and Physically-Based Interpretation of Solar-Induced Vegetation Fluorescence Retrieved From Global Imaging." *Photosynthetica* 59, no. 3: 438–457. https://doi.org/10.32615/ps.2021.034.

Wang, Z., H. Luo, and S. Yang. 2023. "Different Mechanisms for the Extremely Hot Central-Eastern China in July–August 2022 From a Eurasian Large-Scale Circulation Perspective." *Environmental Research Letters* 18, no. 2: 024023. https://doi.org/10.1088/1748-9326/acb3e5.

Wieneke, S., A. Burkart, M. P. Cendrero-Mateo, et al. 2018. "Linking Photosynthesis and Sun-Induced Fluorescence at Sub-Daily to Seasonal Scales." *Remote Sensing of Environment* 219: 247–258. https://doi.org/10.1016/j.rse.2018.10.019.

Wolf, S., T. F. Keenan, J. B. Fisher, et al. 2016. "Warm Spring Reduced Carbon Cycle Impact of the 2012 US Summer Drought." *Proceedings of the National Academy of Sciences* 113, no. 21: 5880–5885. https://doi.org/10.1073/pnas.1519620113.

Xu, H., J. Xiao, and Z. Zhang. 2020. "Heatwave Effects on Gross Primary Production of Northern Mid-Latitude Ecosystems." *Environmental Research Letters* 15, no. 7: 074027. https://doi.org/10.1088/1748-9326/ab8760.

Yamamoto, S. 1970. "Hydrologic Study of Volcano Fuji and Its Adjacent Areas." *Geographical Review Japan* 43, no. 5: 267–284. https://doi.org/10.4157/grj.43.267.

Yang, P., Z. Liu, D. Han, et al. 2025. "Mitigating the Black-Soil Problem in the Reflectance-To-Fluorescence (R2F) Relationship: A Soil-Adjusted Reflectance-Based Approach for Downscaling SIF." *Remote Sensing of Environment* 330: 114998. https://doi.org/10.1016/j.rse.2025.114998.

Yang, P., and C. van der Tol. 2018. "Linking Canopy Scattering of Far-Red Sun-Induced Chlorophyll Fluorescence With Reflectance." *Remote Sensing of Environment* 209: 456–467. https://doi.org/10.1016/j.rse.2018.02.029.

Yang, P., C. van der Tol, P. K. E. Campbell, and E. M. Middleton. 2020. "Fluorescence Correction Vegetation Index (FCVI): A Physically Based Reflectance Index to Separate Physiological and Non-Physiological Information in Far-Red Sun-Induced Chlorophyll Fluorescence." *Remote Sensing of Environment* 240: 111676. https://doi.org/10.1016/j.rse.2020.111676.

Yang, X., J. W. Tang, J. F. Mustard, et al. 2015. "Solar-Induced Chlorophyll Fluorescence That Correlates With Canopy Photosynthesis on Diurnal and Seasonal Scales in a Temperate Deciduous Forest." *Geophysical Research Letters* 42, no. 8: 8. https://doi.org/10.1002/2015gl063201.

Yi, K., R. Li, T. M. Scanlon, M. T. Lerdau, J. A. Berry, and X. Yang. 2024. "Impact of Atmospheric Dryness on Solar-Induced Chlorophyll Fluorescence: Tower-Based Observations at a Temperate Forest." *Remote Sensing of Environment* 306: 114106. https://doi.org/10.1016/j.rse.2024.114106.

Yoshida, Y., J. Joiner, C. Tucker, et al. 2015. "The 2010 Russian Drought Impact on Satellite Measurements of Solar-Induced Chlorophyll Fluorescence: Insights From Modeling and Comparisons With Parameters Derived From Satellite Reflectances." *Remote Sensing of Environment* 166: 163–177. https://doi.org/10.1016/j.rse.2015.06.008.

Zeng, Y. L., G. Badgley, B. Dechant, et al. 2019. "A Practical Approach for Estimating the Escape Ratio of Near-Infrared Solar-Induced Chlorophyll Fluorescence." *Remote Sensing of Environment* 232: 14. https://doi.org/10.1016/j.rse.2019.05.028.

Zweifel, R., K. Steppe, and F. J. Sterck. 2007. "Stomatal Regulation by Microclimate and Tree Water Relations: Interpreting Ecophysiological Field Data With a Hydraulic Plant Model." *Journal of Experimental Botany* 58, no. 8: 2113–2131. https://doi.org/10.1093/jxb/erm050.

Supporting Information

Additional supporting information can be found online in the Supporting Information section. **Figure S1:** The relative comparison between the tower-based system (FHK_QE) and the commercial SIF instrument (FloX; JB hyperspectral, Dusseldorf, Germany). The linear regression equation and the coefficient of determination (R^2) were evaluated. The data was taken in a campaign on June 9, 2022. **Figure S2:** Radiance stability among four different retrieval outputs for solar-induced chlorophyll fluorescence at oxygen A band (SIF O_2A: mW m^{-2} nm^{-1} sr^{-1}). Retrievals include the improved Fraunhofer-line discrimination (iFLD), spectral fitting method (SFM), band shape fitting (BSF), and three-point Fraunhofer-line discrimination (3FLD). The Pearson's correlation coefficient R and p-values between paired variables were evaluated. The equations of the linear regression model were evaluated. Reference links: BSF (https://github.com/Christiaanvandertol/BSF); iFLD and SFM (https://github.com/tommasojulitta/FieldSpectroscopyDP); 3FLD (supplementary materials in Morozumi et al. 2023: https://doi.org/10.1016/j.agrformet.2023.109576). **Figure S3:** Statistical significance (p-value) using Pearson's correlation coefficient among different combinations of the time windows (start and end time). (a, b) Statistics of SIF data, (c, d) statistics of GPP data. (a, c) Combination of Pre-StHW and Late-StHW. (b–d) Combination of Early-StHW and Late-StHW. A darker color indicates a lower p-value. **Figure S4:** Microscope image of a larch needle in a 10×10 lens. There are two lines of dense stomata distribution on the abaxial side of the leaf (small white dots in the image).

Appendix A

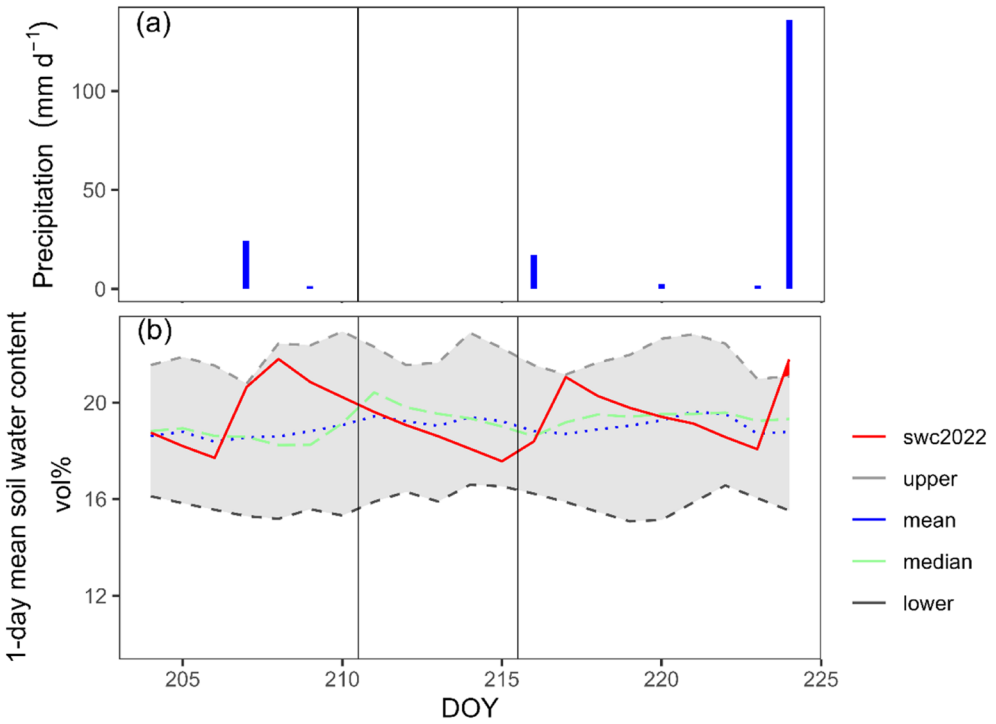


FIGURE A1 | (a) The daily precipitation (blue bar) and (b) the mean and median daily soil water content (volumetric %) from 18 years of data at tower site are plotted (dotted blue and green) with upper and lower 90th percentile thresholds (dashed gray lines). The red line shows the data in 2022. Vertical lines indicate the start and the end of the short heatwave (StHW) period. Horizontal axis is day of the year (DOY).

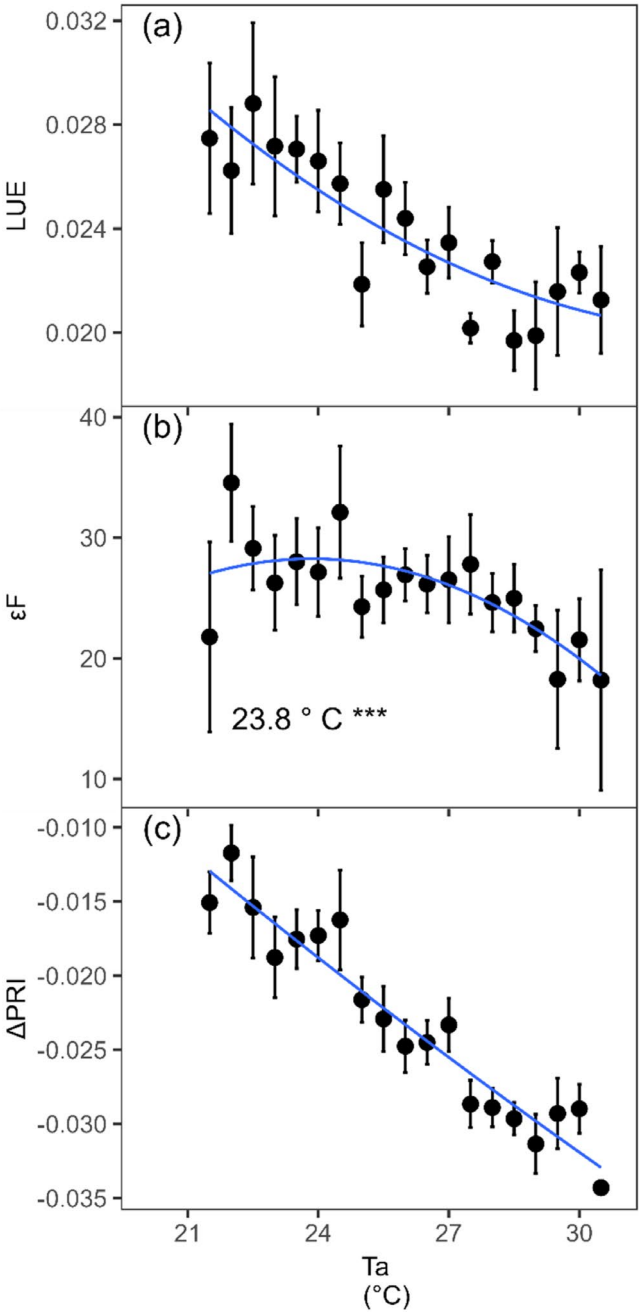


FIGURE A2 | The relationship between air temperature and (a) LUE, (b) εF, and (c) ΔPRI during the study period, DOY 204–224 (including before and after the heatwave period). The data were filtered in APAR > 900 μmol m^{-2}s^{-1} to avoid light-regulated variations. Fitted lines indicate quadratic regressions with optimal temperatures. Asterisks indicate statistical significance (***$p < 0.001$). ΔPRI, delta photochemical reflectance index with dark correction. APAR, absorbed photosynthetically active radiation; DOY, day of the year; LUE, Light use efficiency; εF, canopy fluorescence emission efficiency.

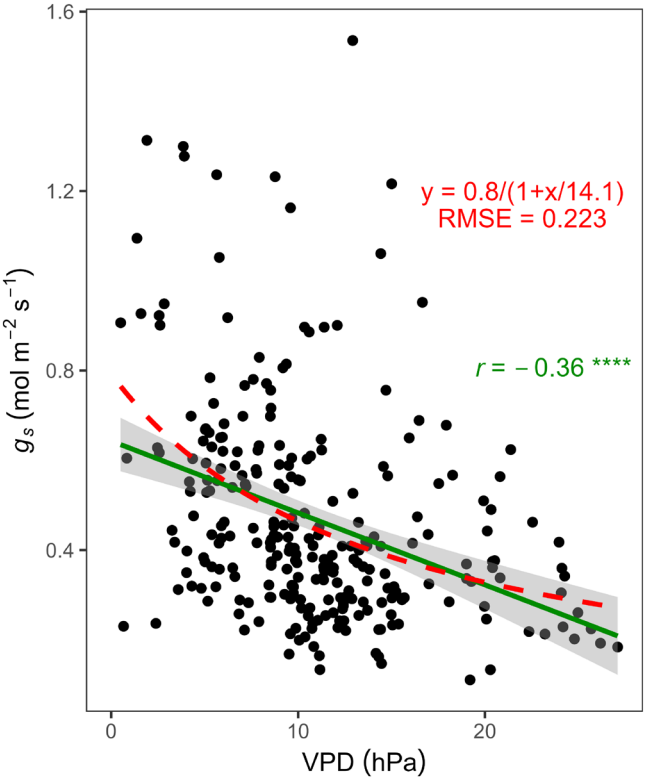


FIGURE A3 | Relationship between canopy conductance (g_s) and vapor pressure deficit (VPD). Lines were fitted for the Lohammar equation (Lohammar et al. 1980) using the non-linear regression and linear regression. The root mean square error (RMSE) and correlation coefficient (r) with p-value (****< 0.0001) are shown.